Harmonic response vs. target orientation: a preliminary study of the effect of polarization on nonlinear junction detection

Gregory Mazzaro, Kyle Gallagher, Kelly Sherbondy, Alex Bouvy, Beatrice Perez, et al.

Gregory Mazzaro, Kyle Gallagher, Kelly Sherbondy, Alex Bouvy, Beatrice Perez, Timothy Pierson, David Kotz, "Harmonic response vs. target orientation: a preliminary study of the effect of polarization on nonlinear junction detection," Proc. SPIE 12108, Radar Sensor Technology XXVI, 1210803 (27 May 2022); doi: 10.1117/12.2617881

SPIE.

Event: SPIE Defense + Commercial Sensing, 2022, Orlando, Florida, United States

Harmonic Response vs. Target Orientation: A Preliminary Study of the Effect of Polarization on Nonlinear Junction Detection

Gregory Mazzaro[1], Kyle Gallagher[2], Kelly Sherbondy[2], Alex Bouvy[3], Beatrice Perez[4], Timothy Pierson[4], and David Kotz[4]

[1]Department of Electrical & Computer Engineering
The Citadel, The Military College of South Carolina
171 Moultrie St, Charleston, SC 29409

[2]United States Army Combat Capabilities Development Command
Army Research Laboratory
2800 Powder Mill Rd, Adelphi, MD 20783

[3]Department of Electrical & Computer Engineering
University of Wisconsin–Madison
1415 Engineering Dr, Madison, WI 53706

[4]Department of Computer Science
Dartmouth College
9 Maynard St, Hanover, NH 03755

ABSTRACT

When an electromagnetically-nonlinear radar target is illuminated by a high-power stepped-frequency probe, a sequence of harmonics is unintentionally emitted by that target. Detection of the target is accomplished by receiving stimulated emissions somewhere in the sequence, while ranging is accomplished by processing amplitude and phase recorded at multiple harmonics across the sequence.

The strength of the harmonics reflected from an electronic target depends greatly upon the orientation of that target (or equivalently, the orientation of the radar antennas). Data collected on handheld wireless devices reveals the harmonic angular-dependence of commercially-available electronics. Data collected on nonlinearly-terminated printed circuit boards implies the origin of this dependency. The results of this work suggest that electronic targets may be classified and ultimately identified by their unique harmonic-response-vs.-angle patterns.

Keywords: radar, harmonic, detection, nonlinear, junction, orientation, polarization

1. INTRODUCTION

The United States Army Research Laboratory (ARL) is currently evaluating radar for the detection and identification of concealed threats such as landmines and other explosives. One non-traditional radar system being developed by ARL addresses handheld electronics which are often used as remote triggers for explosive devices. The developers of this radar intend for it to be small and light enough to be carried by an unmanned aerial vehicle, to fly ahead and provide situational awareness to soldiers entering hazardous environments.

For traditional radar, the frequencies of the waves reflected from the target are the same as (or close to) those transmitted to the target. This type of sensor is known as "linear" radar. Traditional linear wideband radar has proven effective against landmines (buried in sand or soil) and military vehicles (obscured by foliage). It has not proven effective against man-portable electronics. Those electronics (such as a radio or a cell phone) cannot be detected by linear radar because the amount of electromagnetic (EM) energy reflected from them is much smaller than that reflected from nearby clutter. In other words, a linear radar generally cannot "see" an electronic device.

Radar Sensor Technology XXVI, edited by Kenneth I. Ranney, Ann M. Raynal, Proc. of SPIE
Vol. 12108, 1210803 · © 2022 SPIE · 0277-786X · doi: 10.1117/12.2617881

A unique radar being developed by ARL exploits the behavior of junctions formed between dissimilar conductive materials -- a region inherent to all circuit elements containing semiconductors, such as diodes and transistors. Such junctions are distributed throughout every electronic device. When those junctions are illuminated by EM energy at a set of known frequencies, they generate EM energy at frequencies different from those which illuminate them. This behavior is a consequence of EM nonlinearity; thus, systems which exploit this behavior for target detection are called "nonlinear-junction detectors". When range-to-target is computed, these systems are "nonlinear radars".

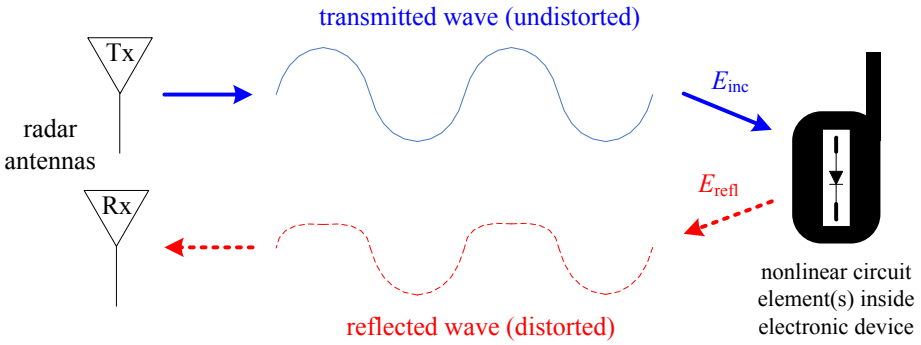

Fig. 1. Nonlinear (junction-detection) radar. The radar antenna transmits an undistorted sinusoidal EM wave towards a target-device, the (nonlinear) electronic device reflects a distorted EM wave back towards the radar, and a second radar antenna captures the reflection. Reception of a distorted wave indicates the presence of an electronic device.

The nonlinear-radar/nonlinear-junction-detection concept is illustrated in Fig. 1. The transmit (Tx) antenna broadcasts an EM wave into an environment which may contain an electronic device. The Tx waveform is illustrated as a single-frequency sinusoid. Let the electric field of the wave incident on the target device be E_{inc}. The semiconductor components of the device capture some of this field and distort it. The distortion may be predicted by [1]

$$E_{\text{refl}}(t) = \sum_{m=1}^{M} a_m E_{\text{trans}}^{m}(t) \tag{1}$$

where E_{refl} is the electric field reflected from the target and a_m are complex power-series coefficients corresponding to the amplitude and phase responses of the target at each harmonic of the original wave E_{inc}. The distorted wave is sensed by the radar receive (Rx) antenna. Reception of the distortion indicates the presence of a semiconductor component, which implies the presence of an electrical circuit which is part of an electronic device.

The choice of transmit waveform is intimately related to the choice of nonlinear response to exploit from the target. The most commonly-exploited response is harmonic [2, 3, 4, 5, 6]. In other words, only a single frequency f_0 is active at any time in the Tx wave, and the received wave consists of integer multiples of this frequency $M{\cdot}f_0$ where M is a positive whole number. Mathematically, the Tx and Rx waveforms may be written [7]

$$E_{\text{trans}}(t) = E_0 \cos(2\pi f_0 \cdot t) \tag{2}$$

$$E_{\text{refl}}(t) = \sum_{M=1}^{\infty} |E_M| \cos\left(2\pi \cdot M f_0 \cdot t + \phi\{E_M\}\right) \tag{3}$$

where E_0 is the amplitude of the transmitted electric field, and $|E_M|$ and $\phi\{E_M\}$ are the amplitude and phase of each harmonic reflected from the nonlinear target.

The entire channel between the transmitter and receiver, including the nonlinear target, has been described in several references. Many derive some version of the nonlinear radar range equation, a variant of the Friis equation extended to a nonlinear receive mode. As an alternative to the aforementioned a_m and E_M coefficients, the nonlinear

power reflected by a target may be quantified by a nonlinear radar-cross-section (RCS) [8]. Thereafter, the nonlinear radar range equation may be written [9, 10, 11]

$$P_R = \frac{M!\left(P_T G_T / M\right)^M G_R \lambda^2 \sigma_M}{\left(4\pi\right)^{M+2} R^{2M+2}} \tag{4}$$

where P_R is received (peak or instantaneous) power, M is the order of the nonlinear interaction, P_T is transmitted power, G_T is the transmit antenna gain, G_R is the receive antenna gain, λ is the transmit wavelength, σ_M is the nonlinear RCS of the target for an M^{th}-order interaction, and R is the distance from the radar to the nonlinear target. Since values of σ_M for electronic targets are small, e.g. 10^{-8} to 10^{-5} m^4/W for $M = 2$ [12], generally a much higher transmit power is required for nonlinear radar to generate a signal-to-noise ratio comparable to that of traditional linear radar at the same distance R.

Although nonlinear reflections from electronic devices are weak, the frequencies produced by these devices (e.g. $2f_0$, $3f_0$) are vastly different from the original transmit set (e.g. f_0 only). In contrast, most materials found in nature are linear, so they do not exhibit this change-of-frequency. Thus, the key advantage of using a nonlinear radar to detect electronic targets-of-interest (compared to using linear radar) is clutter rejection. Recently, nonlinear radar research has grown to support many different applications:

- tracking underground-transported assets [2],
- studying the foraging habits of insects and small amphibians [5, 13],
- performing maritime search-and-rescue [8],
- monitoring human vital signs and movements of limbs [10, 14],
- evaluating the structural integrity of buildings [11, 15],
- tracking radio-frequency (RF) identification tags [16], and
- measuring humidity [17].

Detection of electronics associated with a harmful threat, at an appreciable range, would enable the safe avoidance of the threat. For the Army, the application-of-interest has recently shifted away from detecting electronically-triggered explosive devices alongside a desert road; work now focuses on interrogation of obscured areas and suspicious items along a soldier's driving or walking route, perhaps in an urban environment.

Identification of an electronic target might enable the deactivation and/or removal of a threat. Working towards that end, researchers have suggested sweeping transmit power and developing signatures of electronic targets from their characteristic P_R-vs.-P_T curves [1, 18]. Data presented in this paper indicates that the strength of a harmonic reflected from an electronic target depends greatly upon the orientation of that target; thus, it may be possible to identify electronic targets from their unique response-vs.-angle patterns.

2. EXPERIMENTAL NONLINEAR RADAR

Researchers at ARL have constructed radars which operate in both the linear and nonlinear modes [19]. In a recent embodiment, the radar transmission steps continuously through a sequence of frequencies, increasing from a start frequency of 600 MHz to an end frequency of 680 MHz with an even step spacing of 500 kHz. For this work, the electronic target-devices were placed in front of the Tx/Rx antennas (i.e. with clear line-of-sight), the positions of the antennas were fixed, and each target was rotated a full 360º in even steps. At each step around its rotation, the target was illuminated with a radar wave and its harmonic response was captured.

A picture of the radar's transceiver is shown in Fig. 2. The unit transmits 100-µs-long constant-amplitude stepped-frequency pulses. The transceiver is controlled by a desktop computer running LabView. The National Instruments USRP-2954R software-defined radio ("SDR" in the figure) generates and captures the stepped-frequency pulses. The custom Tx power-amplifier set ("PAs" in the figure) boosts the low-power waveform generated by the SDR to approximately 25 dBm (fed directly into the Tx antenna). The custom Rx low-noise-amplifier set ("LNAs" in the figure) boosts the weak target response by approximately 27 dB in the 2nd-harmonic band (1200 MHz to 1460 MHz) before it is digitized by the SDR. The Tx amp is powered by two external supplies (12 VDC and 5 VDC), while the Rx amp is powered by a single external (5 VDC) supply.

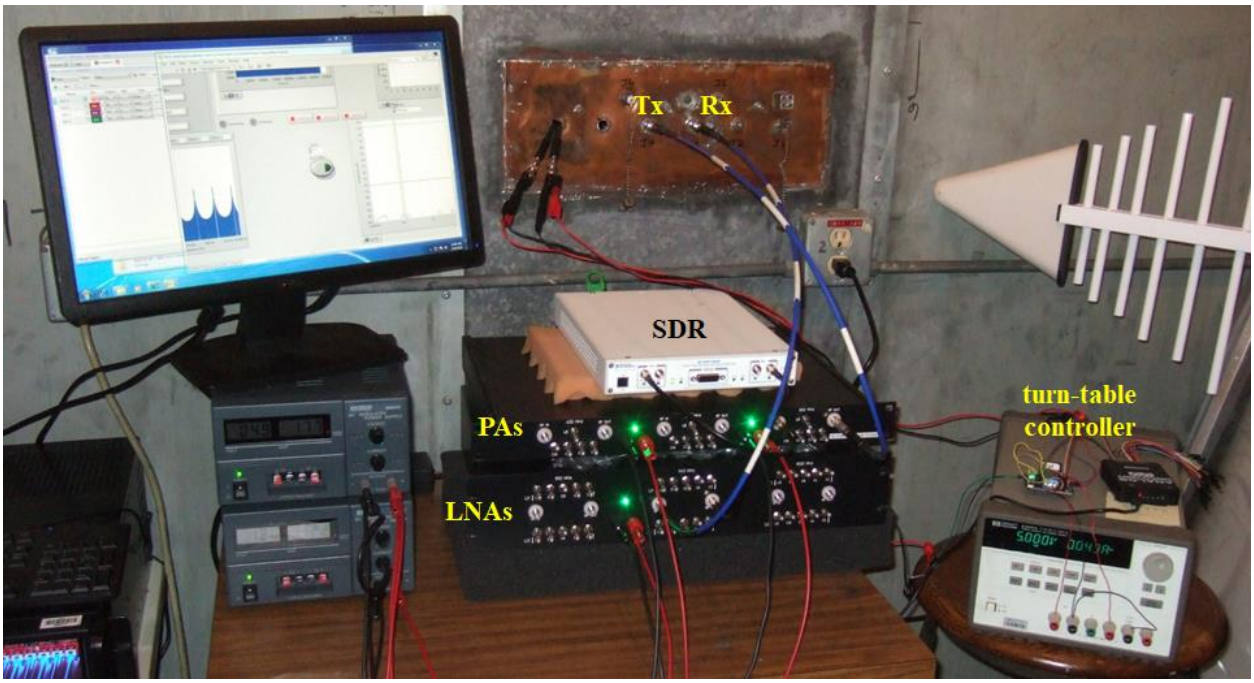

Fig. 2. Nonlinear radar controller, signal generator/capture unit, custom amplifiers, and turntable controller.

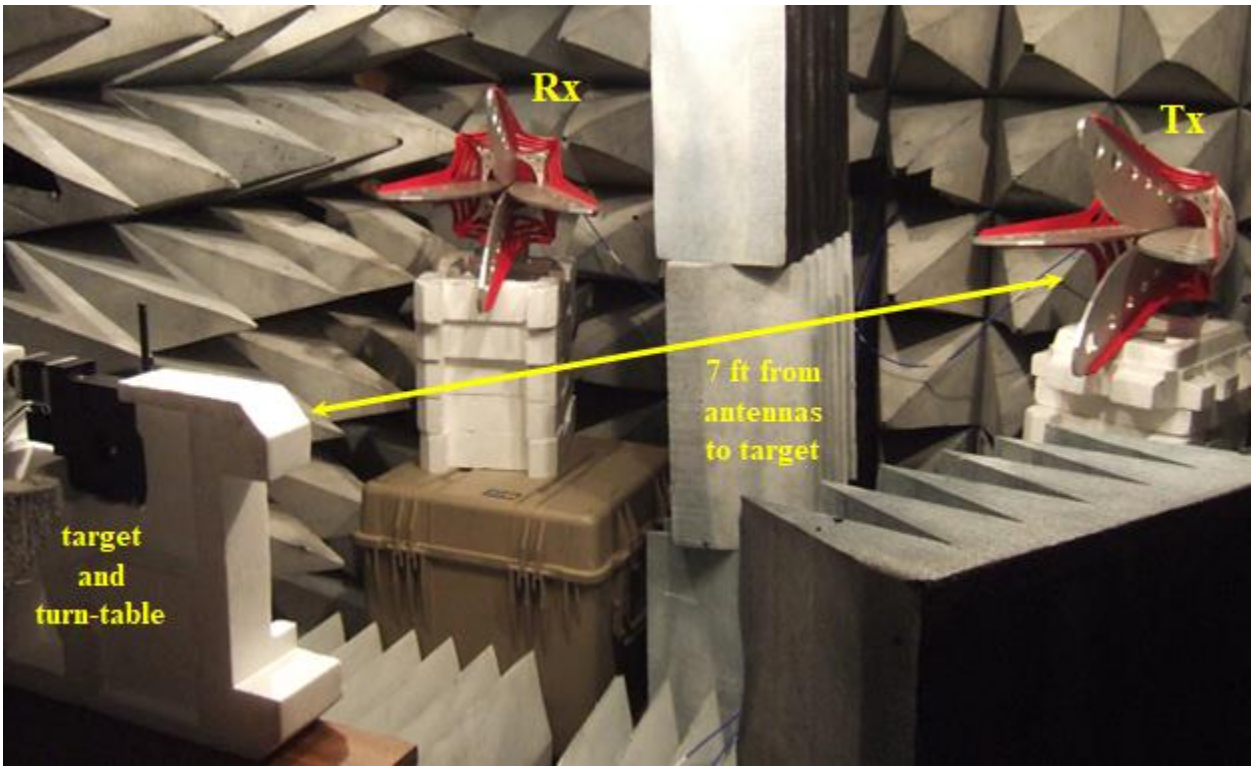

Fig. 3. Target-device location, in front of the wideband horn antennas.

The SDR captures the amplitude and phase of each received harmonic (relative to each amplitude and phase of the original transmit probe), and LabView performs an inverse Fourier Transform of the harmonic transfer function to form a radar-range-profile for each target orientation. Without a target present, the peak harmonic pulse recorded by the SDR is approximately –90 dBm, which represents the harmonic noise floor of this experiment. Within each profile, a peak appearing well above the noise floor indicates the presence of the target. When the profile is mapped against distance (away from the Tx/Rx antennas), a distinct global peak indicates the location of the target. Within each data figure presented in this report, only the (global) maximum value of each harmonic range-profile is plotted.

A picture of the Tx/Rx antenna pair and the target emplacement is given in Fig. 3. The Tx and Rx antennas are both ETS Lindgren 3164-06 wideband horns. Each has two feed ports: one for vertical (V) polarization and another for horizontal (H) polarization. Two combinations (VV, VH) were tested for each target. The target was placed 7 ft in front of the Tx/Rx antennas, and the Tx/Rx antennas themselves were spaced apart by 4 ft (with radio-frequency-absorbing panels placed in-between, as seen in the figure).

Fig. 4 is a front view of the platform to which each target was attached for the "clock-rotation" experiment. A narrow wooden platform is attached to a 4-inch-diameter worm-gear optical turntable. The turntable and platform are spun by a 5-V stepper motor, powered through a SeeedStudio L298 H-Bridge Motor Driver, with logic pulses provided by a Digilent Analog Discovery prototyping instrument. The turntable itself is visible in Fig. 4, while the motor driver board and Analog Discovery instrument are visible along the right side of Fig. 2.

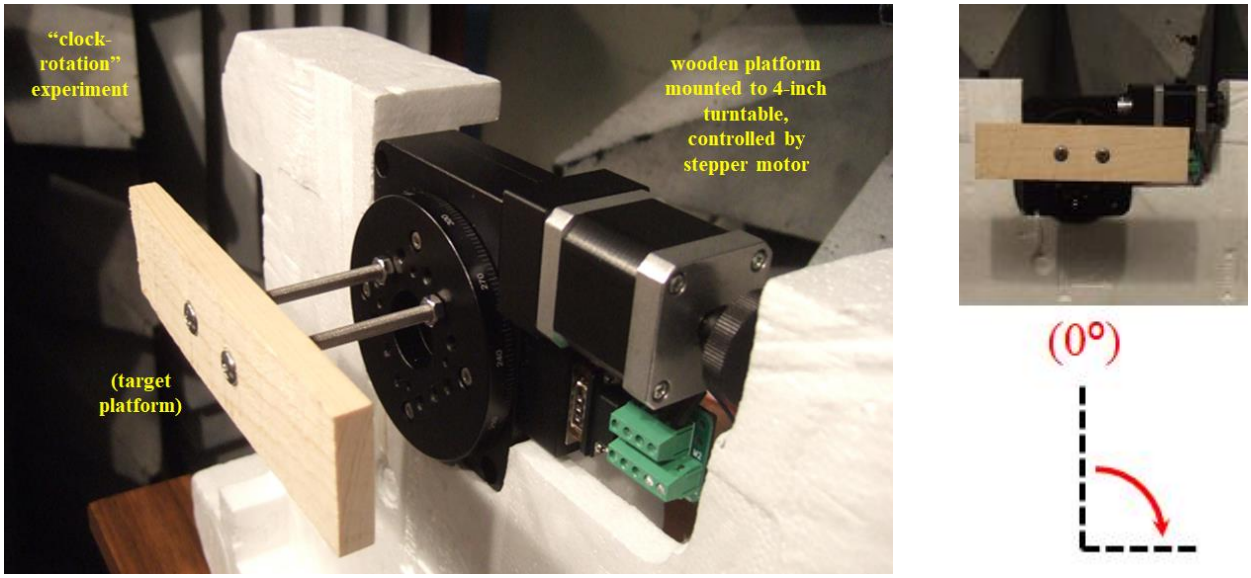

Fig. 4. Nonlinear-target-rotation experiment: the target is "rotated like a clock" when attached to the front of the narrow-wooden plank. Behind the wood, a 4-inch turntable is rotated by a stepper motor.

Fig. 5 shows how the turntable was re-oriented to be horizontally flat (level), with a different Styrofoam piece mounted on top to hold each target, for the "top-spin" experiment. Again the platform was rotated a full 360º for each target (and each arrangement of its antenna).

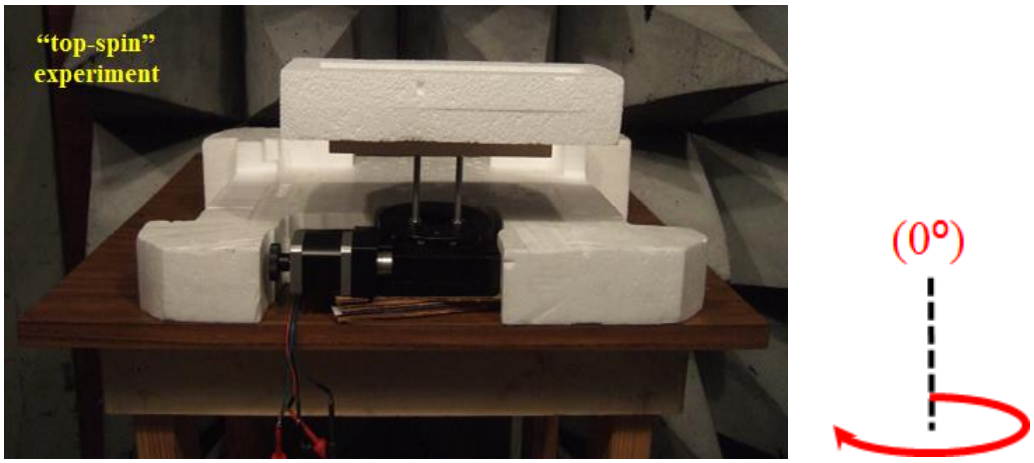

Fig. 5. Nonlinear-target-rotation experiment: target is "spun like a top" when placed on/in the Styrofoam platform (attached to the narrow wooden plank). Beneath the Styrofoam, the platform is rotated by the stepper motor.

The following two sections amount to a catalogue of data recorded from two commercially-available smart light-bulbs, two handheld radios, those same radios with their antennas removed, two remote-controlled (RC) toy-tank transmitters, and those same transmitters with their antennas removed. Within each plot is peak-harmonic-signal-strength vs. rotation-angle. The first set of data is collected from targets "rotated like a clock" when looking from the Tx/Rx antennas towards the target; the second set is collected from targets "spun like a top" (clockwise when looking down on the targets from above). The original starting position of each target is the same across the two experiments, and the center-of-mass of each target is at approximately the same location across all permutations of targets and rotation angles.

3. EXPERIMENT: CLOCK-ROTATION

Figs. 6–16 contain a picture of each target-device next to the peak of each target's 2nd-harmonic range profile, plotted against angle across a 360º rotation of the platform seen in Fig. 4. Each data point corresponds to a new range-profile peak, recorded in 5º increments (for a total of 72 data points within each plot).

The data of Fig. 6 was recorded for the "no-target" (empty platform) case. Fig. 7 was recorded from a Linkind Smart WiFi-controllable light bulb. Fig. 8 was recorded from a similar bulb manufactured by TJOY. In Fig. 9 is the Motorola MD200R family-radio-service (FRS) radio; in Fig. 10 is the MD200R radio with its antenna replaced by a 50-Ω termination. Fig. 11 contains data recorded from a Uniden GMR1636-2C FRS radio; similarly, in Fig. 12 is the GMR1636 radio with its antenna replaced by 50 Ω. Fig. 13 was recorded from a 27-MHz transmitter for an RC toy tank; in Fig. 14 is the same transmitter with its antenna removed (i.e. open-circuited). Figs. 15 and 16 contain data from a 49-MHz RC transmitter, with and without its antenna attached, respectively.

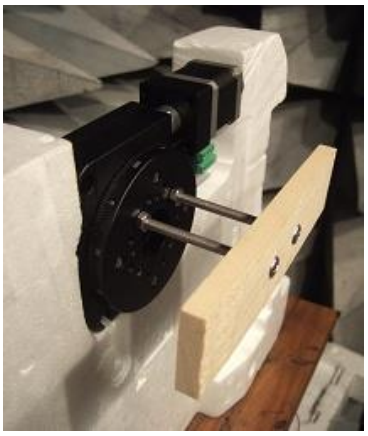

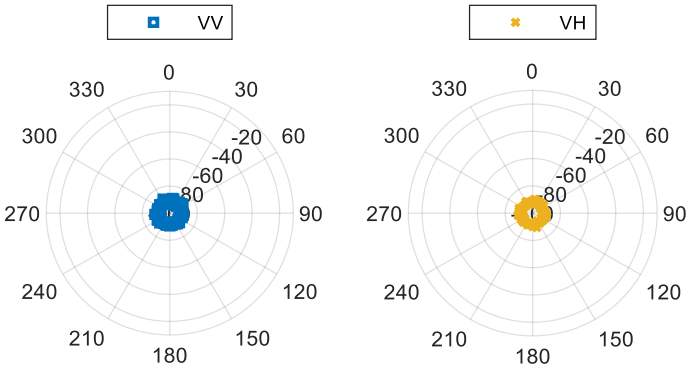

Fig. 6. No target, platform rotated clockwise: (a) picture, as placed in front of the radar antennas, (b) peak-radar-pulse amplitude vs. angle for VV and VH polarizations; outer axis labels are in degrees; inner labels are in dBm.

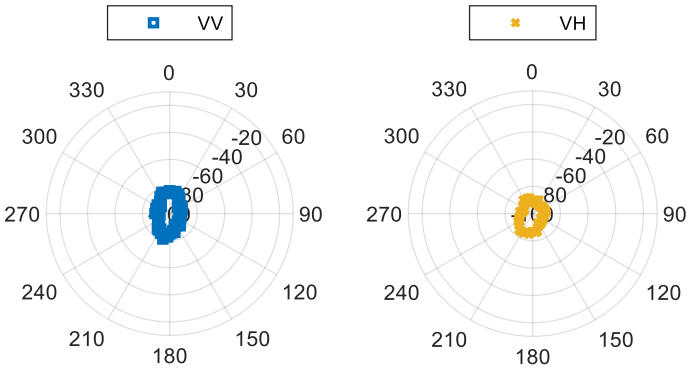

Fig. 7. Linkind smart light-bulb, rotated clockwise: (a) picture of the target, as seen from the antennas, (b) peak-pulse amplitude vs. angle for VV and VH polarizations; outer axis labels are in degrees; inner labels are in dBm.

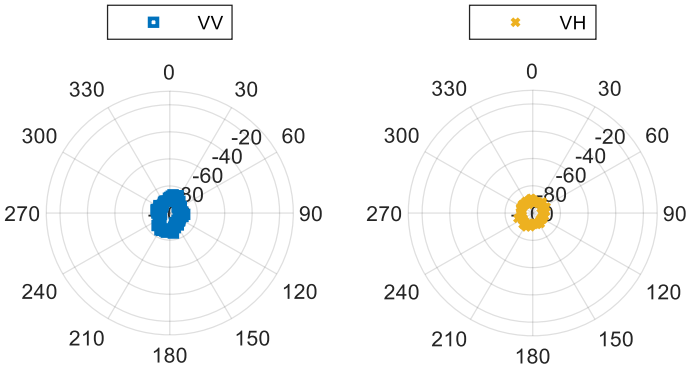

Fig. 8. TJOY smart light-bulb, rotated clockwise: (a) picture of the target, as seen from the antennas, (b) peak-pulse amplitude vs. angle for VV and VH polarizations; outer axis labels are in degrees; inner labels are in dBm.

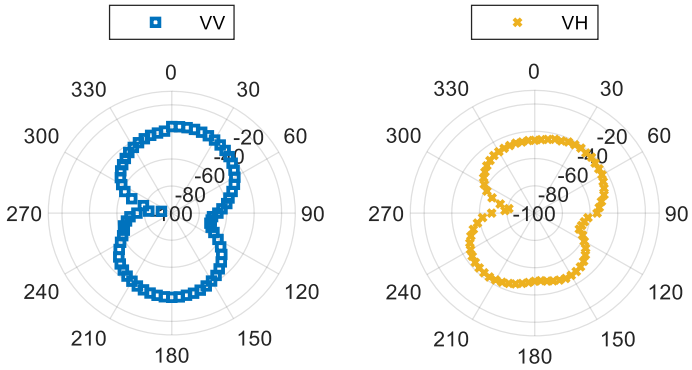

Fig. 9. Motorola MD200R radio, rotated clockwise: (a) picture of the target, as seen from the antennas, (b) peak-pulse amplitude vs. angle for VV and VH polarizations; outer axis labels are in degrees; inner labels are in dBm.

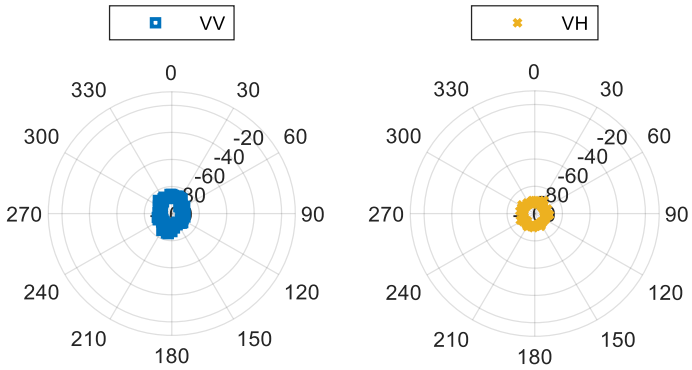

Fig. 10. Motorola MD200R radio with its antenna port terminated in 50 Ω, rotated clockwise: (a) picture of the target, (b) peak-amplitude vs. angle for VV and VH polarizations; outer axis labels are in degrees; inner labels are in dBm.

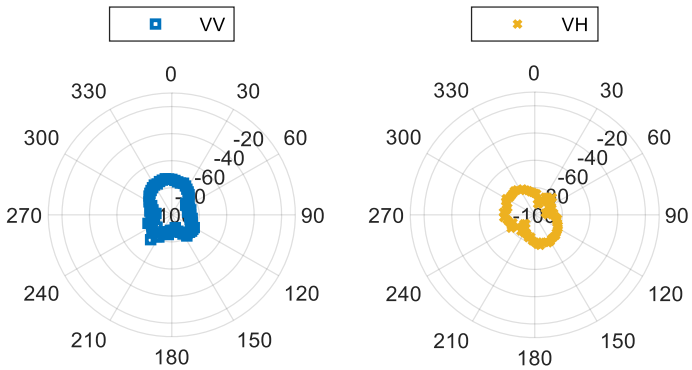

Fig. 11. Uniden GMR1636-2C radio, rotated clockwise: (a) picture of the target, as seen from the antennas, (b) peak-pulse amplitude vs. angle for VV and VH polarizations; outer axis labels are in degrees; inner labels are in dBm.

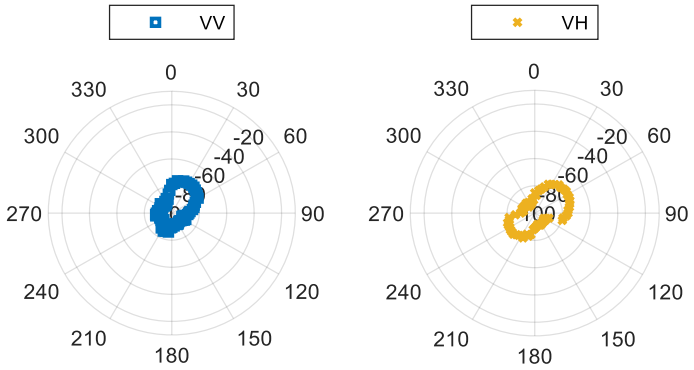

Fig. 12. Uniden GMR1636-2C with its antenna port terminated in 50 Ω, rotated clockwise: (a) picture, as seen from the antennas, (b) peak-amplitude vs. angle for VV and VH; outer axis labels are in degrees; inner labels are in dBm.

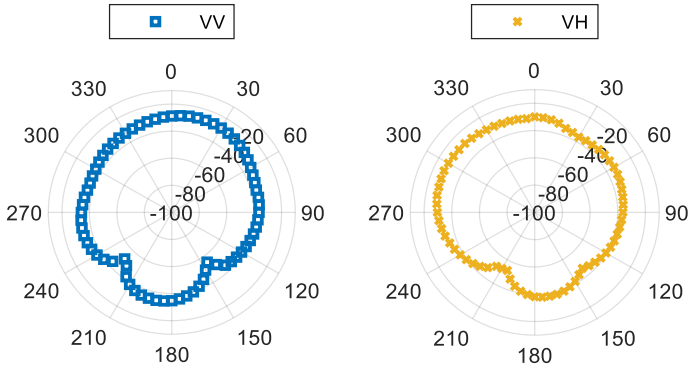

Fig. 13. 27-MHz remote-controlled toy tank transmitter, rotated clockwise: (a) picture of the target, (b) peak-pulse amplitude vs. angle for VV and VH polarizations; outer axis labels are in degrees; inner labels are in dBm.

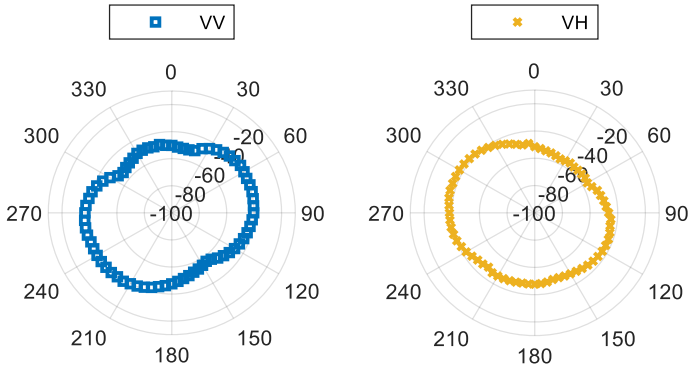

Fig. 14. 27-MHz RC toy tank transmitter with antenna removed, rotated clockwise: (a) picture of the target, (b) peak-pulse amplitude vs. angle for VV and VH polarizations; outer axis labels are in degrees; inner labels are in dBm.

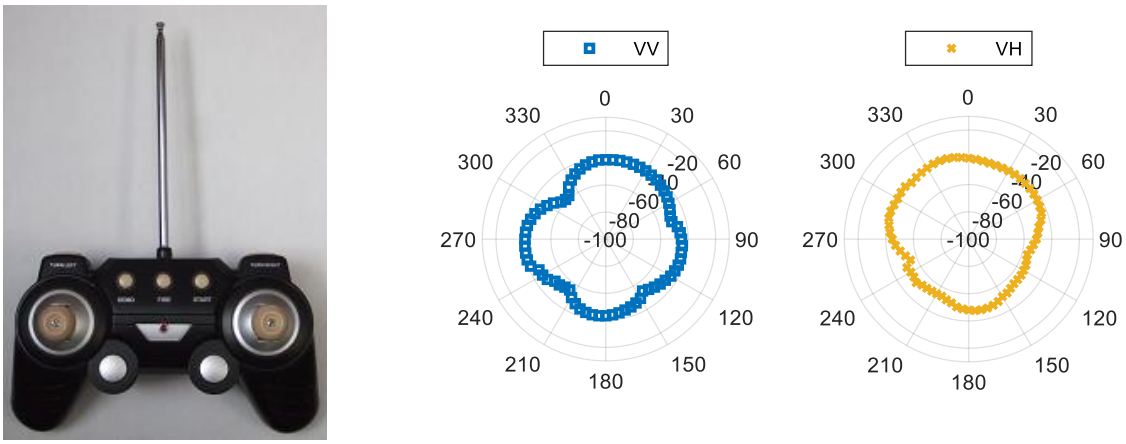

Fig. 15. 49-MHz remote-controlled toy tank transmitter, rotated clockwise: (a) picture of the target, (b) peak-pulse amplitude vs. angle for VV and VH polarizations; outer axis labels are in degrees; inner labels are in dBm.

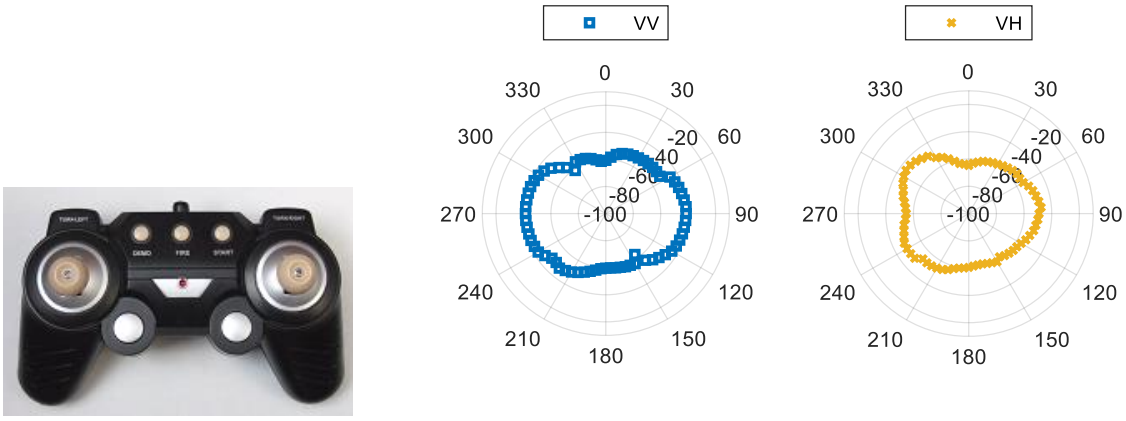

Fig. 16. 49-MHz RC toy tank transmitter with antenna removed, rotated clockwise: (a) picture of the target, (b) peak-pulse amplitude vs. angle for VV and VH polarizations; outer axis labels are in degrees; inner labels are in dBm.

	radar orientation & statistic:			
target:	**VV, mean**	**VV, SD**	**VH, mean**	**VH, SD**
no target -- empty platform	–91 dBm	1 dB	–91 dBm	1 dB
Linkind wifi smart light bulb	–89 dBm	3 dB	–90 dBm	3 dB
TJOY wifi smart light bulb	–90 dBm	2 dB	–91 dBm	1 dB
MD200R radio, with antenna	–51 dBm	13 dB	–51 dBm	9 dB
MD200R radio, antenna terminated	–90 dBm	2 dB	–91 dBm	1 dB
GMR1636 radio, with antenna	–82 dBm	5 dB	–83 dBm	4 dB
GMR1636 radio, antenna terminated	–87 dBm	6 dB	–84 dBm	7 dB
27-MHz RC transmitter, with antenna	–36 dBm	6 dB	–36 dBm	6 dB
27-MHz RC transmitter, no antenna	–45 dBm	6 dB	–46 dBm	6 dB
49-MHz RC transmitter, with antenna	–46 dBm	4 dB	–47 dBm	6 dB
49-MHz RC transmitter, no antenna	–50 dBm	7 dB	–55 dBm	5 dB

Table I. Mean and standard-deviation of radar-range-profile peak, across all angles for “clock-rotation” experiment.

The mean and standard-deviation of each peak-amplitude trace, for each target and each radar-antenna orientation, are listed in Table I. The "noise floor" of this experiment is the mean of the "no target" case, –91 dBm for both VV and VH orientations. The Linkind bulb is barely detectable and the TJOY bulb is not detectable. The MD200R radio is detectable above the noise floor (by 40 dB) but its response drops into the noise floor when its antenna is terminated. The GMR1636 radio is weak but detectable (by 8-9 dB above the noise) with its antenna and it is weaker but still detectable (by 4-7 dB above the noise) when its antenna is terminated. The two RC-tank transmitters are stronger and display the same trend as the GMR1636: the 27-MHz unit is very detectable (by 55 dB) with its antenna and still detectable (by 45 dB) with its antenna removed; the 49-MHz transmitter is consistently about 10 dB weaker than the 27-MHz unit.

The shapes traced by the MD200R and GMR1636 radios resemble ideal dipole-antenna patterns [20]. Since the harmonics received from of each device drop considerably when its antenna is terminated, it is reasonable to conclude that the nonlinear response is generated largely by the RF front-end including the antenna. The shapes traced by the 27- and 49-MHz RC transmitters roughly resemble the pattern of a dipole antenna near a ground plane [21]. When each antenna is removed, the response does not drop into the noise, and the antenna-pattern elongates along 90º/270º rather than 0º/180º. This behavior indicates that it is not only the RF front-end of the device that is producing the nonlinear response; it appears that the layout of the device's printed circuit board (PCB) contributes significantly to its angular dependence.

With the exception of the 27- and 49-MHz RC transmitters, when each target is detectable, the response is strongest when the polarization of the target antenna aligns with the polarization of the radar transmit antenna. Since the mean response of VV and VH is within 5 dB for all targets and antenna arrangements, there appears to be no advantage (or disadvantage) to orienting the radar receive antenna vertically or horizontally.

4. EXPERIMENT: TOP-SPIN

Figs. 17–27 parallel the photos and data plots of Figs. 6–16, but now each target "spins like a top" instead of "rotating like a clock".

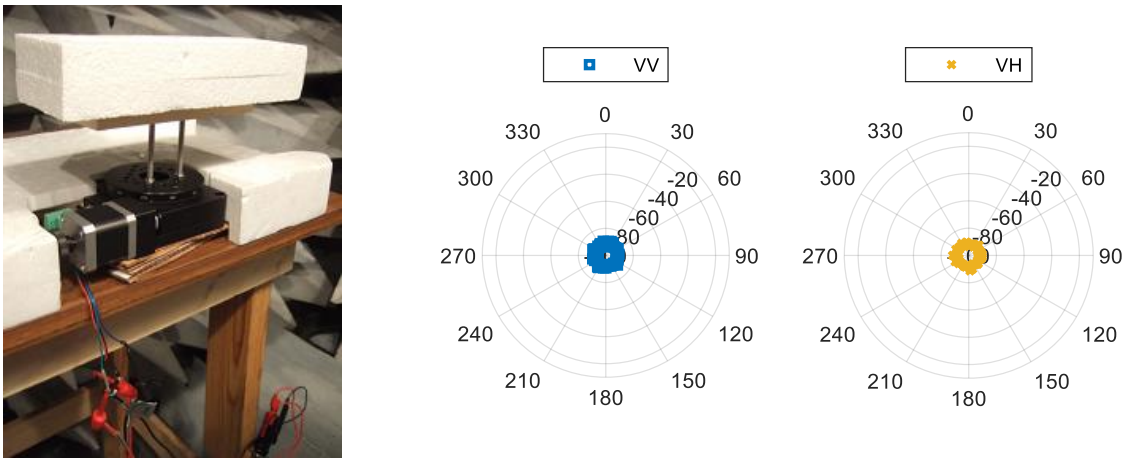

Fig. 17. No target, platform spun clockwise (as seen from above): (a) picture, as placed in front of the antennas, (b) peak-pulse amplitude vs. angle for VV and VH polarizations; outer axis labels are in degrees; inner labels are in dBm.

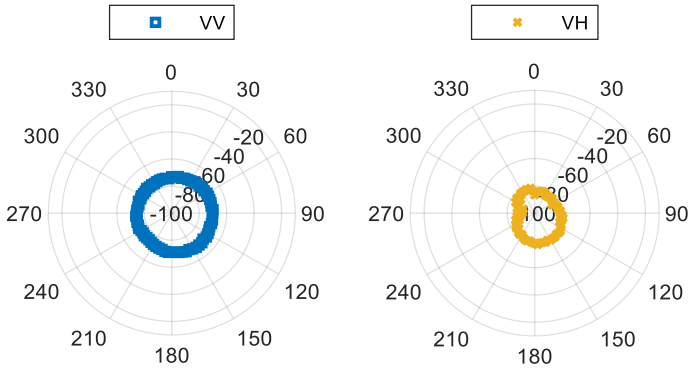

Fig. 18. Linkind smart light-bulb, spun clockwise: (a) picture of the target, as seen from the antennas, (b) peak-pulse amplitude vs. angle for VV and VH polarizations; outer axis labels are in degrees; inner labels are in dBm.

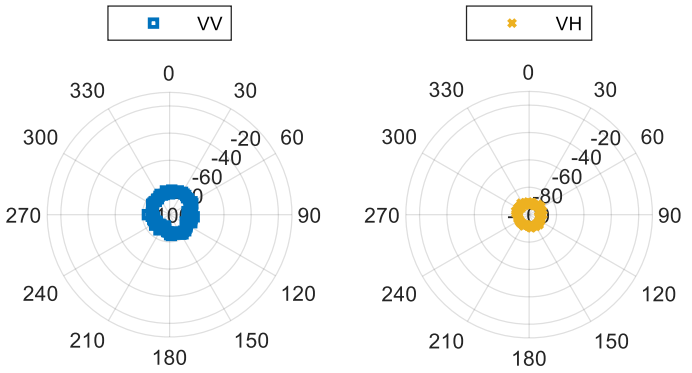

Fig. 19. TJOY smart light-bulb, spun clockwise: (a) picture of the target, as seen from the antennas, (b) peak-pulse amplitude vs. angle for VV and VH polarizations; outer axis labels are in degrees; inner labels are in dBm.

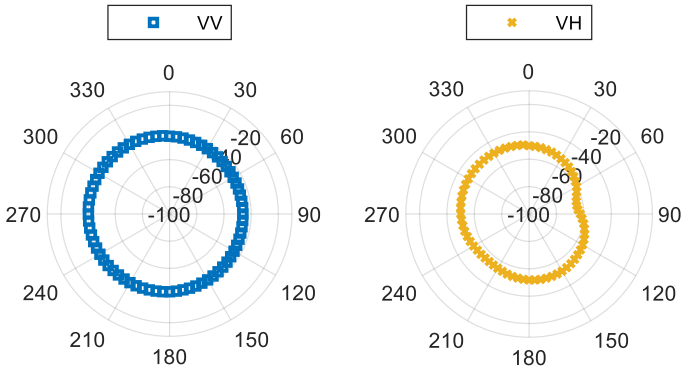

Fig. 20. Motorola MD200R radio, spun clockwise: (a) picture of the target, as seen from the antennas, (b) peak-pulse amplitude vs. angle for VV and VH polarizations; outer axis labels are in degrees; inner labels are in dBm.

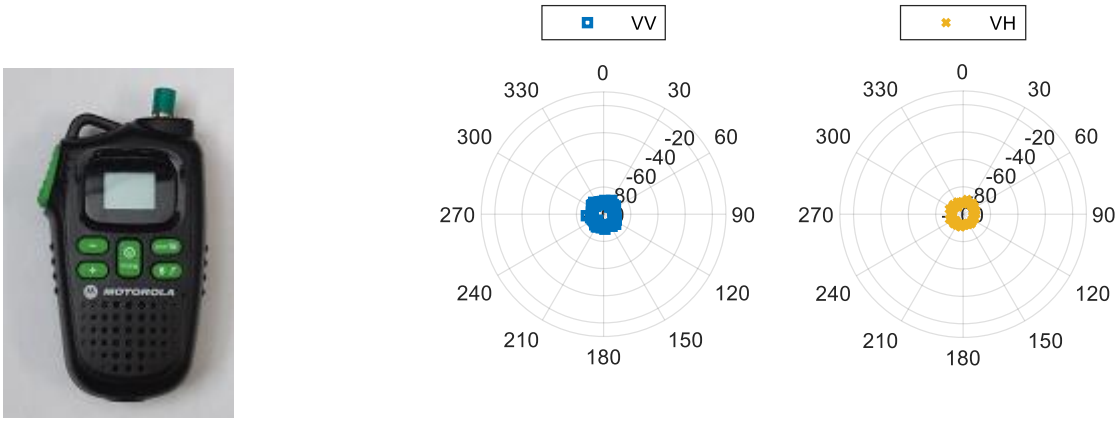

Fig. 21. Motorola MD200R radio with its antenna port terminated in 50 Ω, spun clockwise: (a) picture of the target, (b) peak-amplitude vs. angle for VV and VH polarizations; outer axis labels are in degrees; inner labels are in dBm.

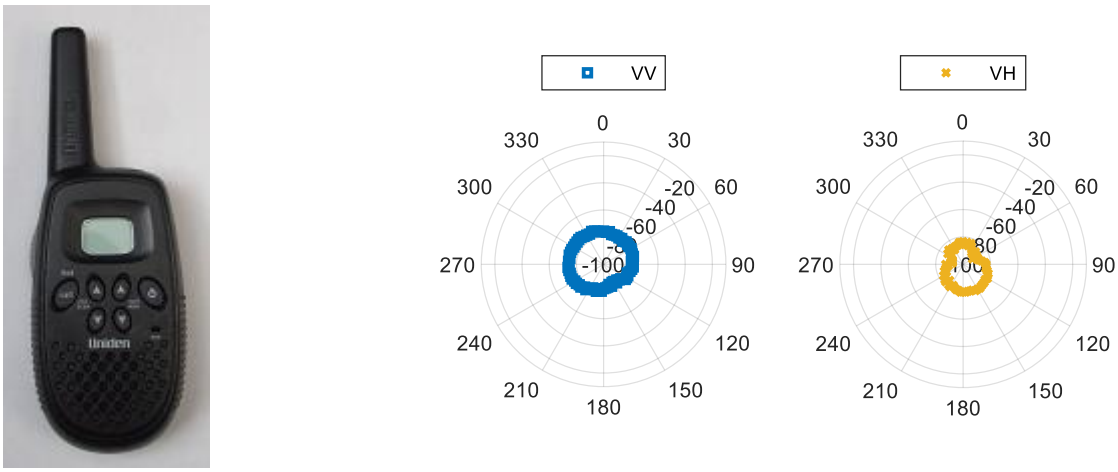

Fig. 22. Uniden GMR1636-2C radio, spun clockwise: (a) picture of the target, as seen from the antennas, (b) peak-pulse amplitude vs. angle for VV and VH polarizations; outer axis labels are in degrees; inner labels are in dBm.

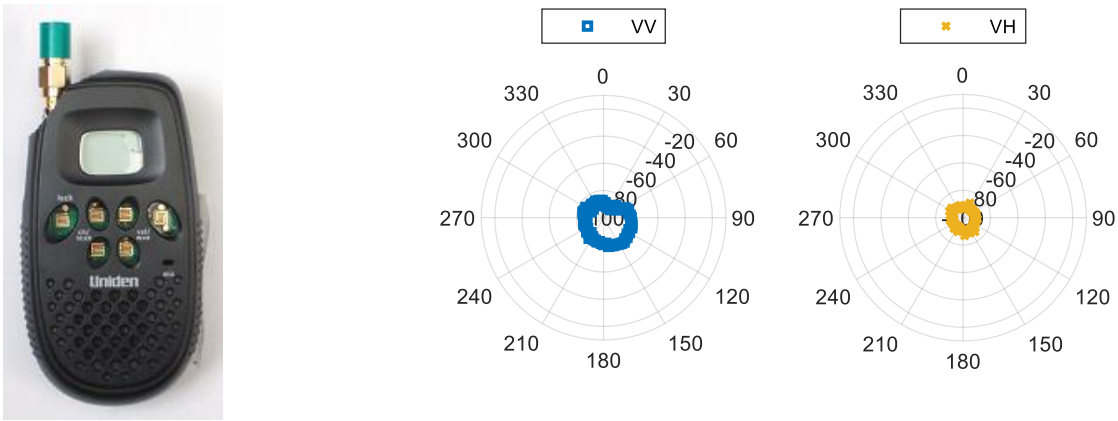

Fig. 23. Uniden GMR1636-2C with its antenna port terminated in 50 Ω, spun clockwise: (a) picture, as seen from the antennas, (b) peak-amplitude vs. angle for VV and VH; outer axis labels are in degrees; inner labels are in dBm.

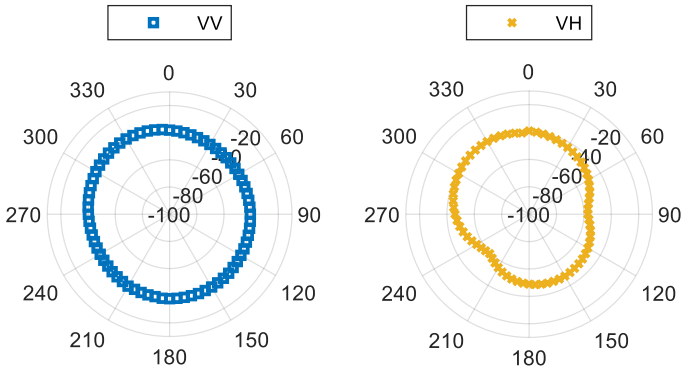

Fig. 24. 27-MHz remote-controlled toy tank transmitter, spun clockwise: (a) picture of the target, (b) peak-pulse amplitude vs. angle for VV and VH polarizations; outer axis labels are in degrees; inner labels are in dBm.

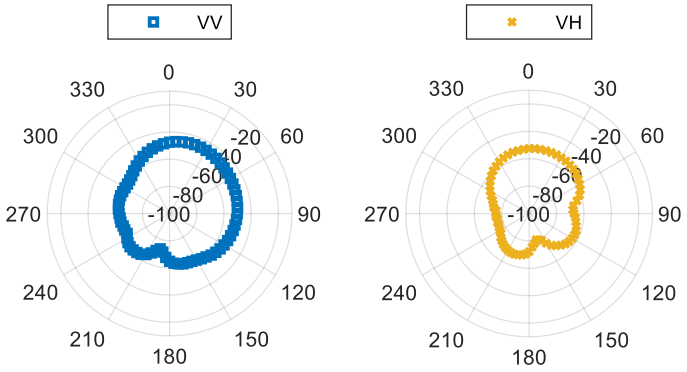

Fig. 25. 27-MHz RC toy tank transmitter with antenna removed, spun clockwise: (a) picture of the target, (b) peak-pulse amplitude vs. angle for VV and VH polarizations; outer axis labels are in degrees; inner labels are in dBm.

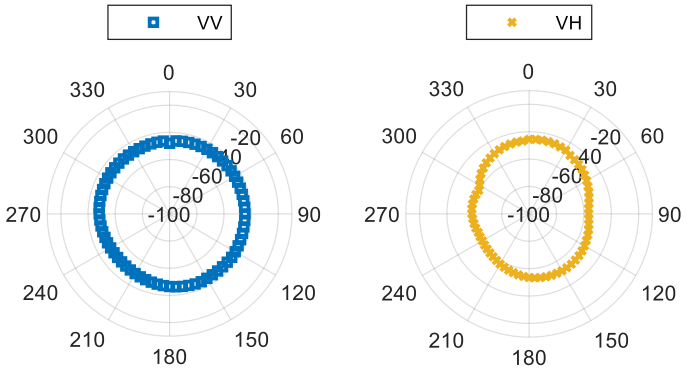

Fig. 26. 49-MHz remote-controlled toy tank transmitter, spun clockwise: (a) picture of the target, (b) peak-pulse amplitude vs. angle for VV and VH polarizations; outer axis labels are in degrees; inner labels are in dBm.

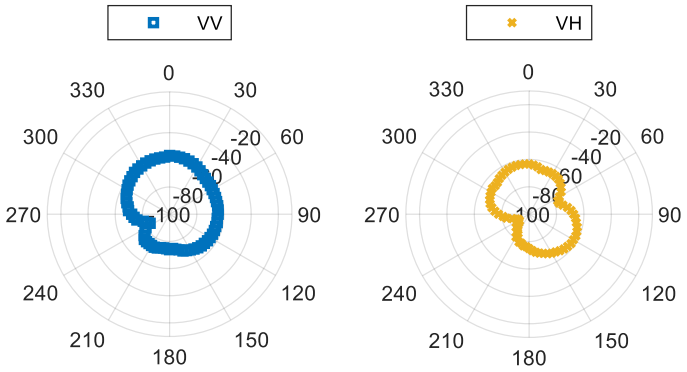

Fig. 27. 49-MHz RC toy tank transmitter with antenna removed, spun clockwise: (a) picture of the target, (b) peak-pulse amplitude vs. angle for VV and VH polarizations; outer axis labels are in degrees; inner labels are in dBm.

	radar orientation & statistic:			
target:	**VV, mean**	**VV, SD**	**VH, mean**	**VH, SD**
no target -- empty platform	–91 dBm	1 dB	–91 dBm	1 dB
Linkind wifi smart light bulb	–72 dBm	2 dB	–83 dBm	4 dB
TJOY wifi smart light bulb	–85 dBm	3 dB	–91 dBm	1 dB
MD200R radio, with antenna	–43 dBm	2 dB	–53 dBm	4 dB
MD200R radio, antenna terminated	–91 dBm	1 dB	–91 dBm	1 dB
GMR1636 radio, with antenna	–78 dBm	3 dB	–85 dBm	4 dB
GMR1636 radio, antenna terminated	–84 dBm	5 dB	–91 dBm	1 dB
27-MHz RC transmitter, with antenna	–39 dBm	2 dB	–48 dBm	6 dB
27-MHz RC transmitter, no antenna	–57 dBm	7 dB	–65 dBm	9 dB
49-MHz RC transmitter, with antenna	–47 dBm	2 dB	–54 dBm	5 dB
49-MHz RC transmitter, no antenna	–67 dBm	7 dB	–72 dBm	8 dB

Table II. Mean and standard-deviation of radar-range-profile peak, across all angles for “top-spin” experiment.

Much like Table I for the “clock-rotation” experiment, Table II lists the mean and standard-deviation for all targets and antenna arrangements in the “top-spin” experiment. As before, most targets are detectable above the noise floor. The cases which were not detectable were (a) the TJOY bulb with antennas in the VH orientation, (b) the MD200R radio with its antenna terminated, in both VV and VH orientations, and (c) the GMR1636 radio with its antenna terminated, in the VH orientation.

Compared to the standard-deviations for the “clock-rotation” experiment (5-13 dB when the target is detectable), the deviations of the light bulbs and radios for the “top-spin” experiment were generally much smaller (2-5 dB when detectable); this behavior is to be expected if the target’s antenna (+ RF front-end) is primarily responsible for generating its nonlinear response, since the antennas are cylindrically symmetric. The standard-deviations of the RC transmitters are comparable and slightly higher for the “top-spin” experiment; this trend is also expected given that the target’s PCB contributes significantly to the nonlinear response. There are rotation angles for which the PCB is not facing the Tx/Rx antennas, i.e. the incoming wave shears across the target and does not couple strongly onto (or off of) the PCB. This dip in generation of the harmonics is visible in Figs. 25 and 27 as a tightening of the patterns near 90º/270º.

5. HARDWARE MODELING

To better understand the origin of the harmonic responses generated by RF-electronic targets, a simple hardware model for an RF front-end was assembled. If the harmonic responses recorded from this model match those recorded from actual electronic devices, additional experiments may be conducted on the model to gain insight into how such responses may be maximally stimulated to optimize target detection. Such testing would obviate the need to disassemble manufactured devices to test electronic sub-systems. Such disassembly is often destructive for products whose electronics are integrated on a single circuit board.

The basic RF-front-end model is shown in Fig. 28; it consists of a (bendable) dipole antenna attached with an SMA connector to a piece of perf-board. The perf-board contains a single copper-tape trace along its top-side (visible in the figure) and another copper-tape trace running parallel to the first on the opposite side of the board (not visible in this figure). The SMA connector at the edge of the perf-board opposite the antenna connects to the input of a MiniCircuits FK-3000+ frequency doubler which acts as a nonlinear junction. The output of the doubler is terminated in 50 Ω.

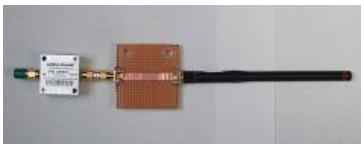

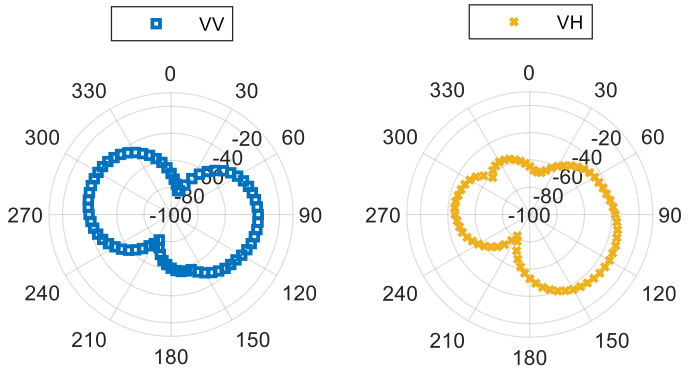

Fig. 28. NLJ + 2-inch PCB + straight antenna, rotated clockwise: (a) picture of the target, as seen from the antennas, (b) peak-amplitude vs. angle for VV and VH; outer axis labels are in degrees; inner labels are in dBm.

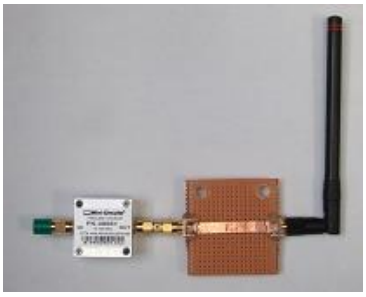

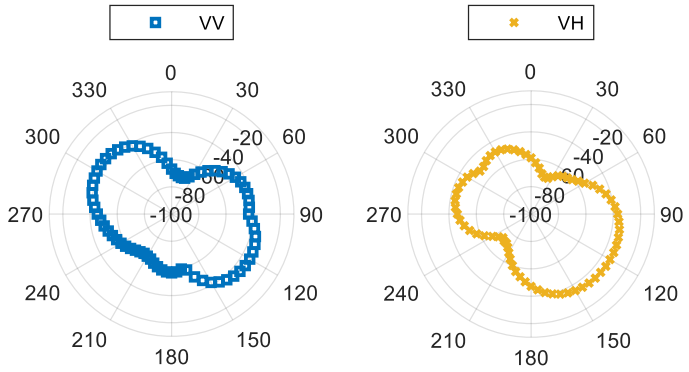

Fig. 29. NLJ + 2-inch PCB + bent antenna, rotated clockwise: (a) picture of the target, as seen from the antennas, (b) peak-amplitude vs. angle for VV and VH; outer axis labels are in degrees; inner labels are in dBm.

The data of Figs. 28 and 29 demonstrate that the doubler + 2-inch PCB + antenna assembly functions adequately as a nonlinear target: it generates harmonics of a similar order-of-magnitude to the targets of Figs. 6–27. Also the harmonics received are preferential to the alignment of the PCB with the radar's Tx antenna.

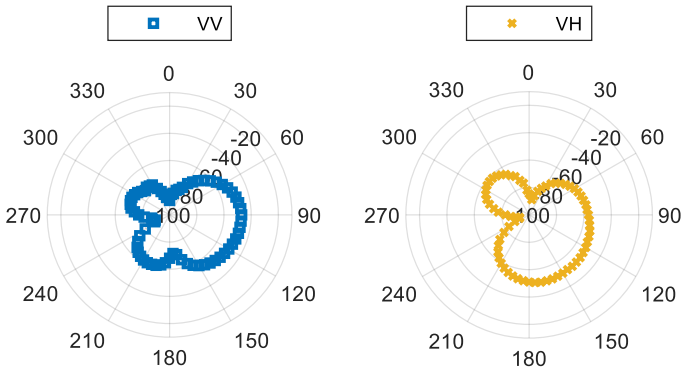

Fig. 30. NLJ + 4-inch PCB + straight antenna, rotated clockwise: (a) picture of the target, as seen from the antennas, (b) peak-amplitude vs. angle for VV and VH; outer axis labels are in degrees; inner labels are in dBm.

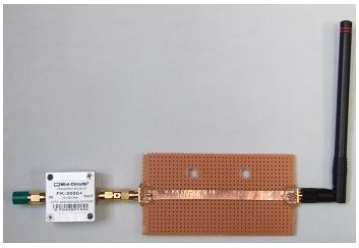

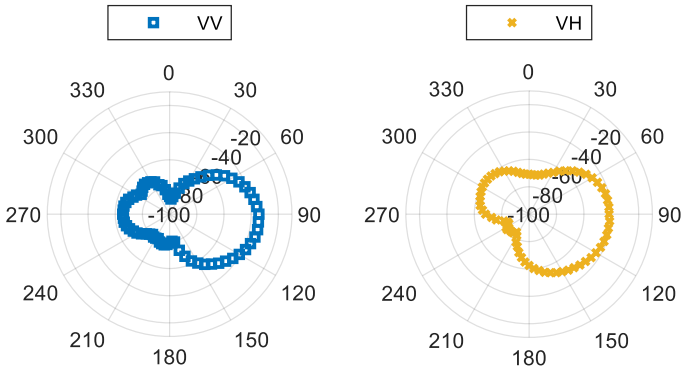

Fig. 31. NLJ + 4-inch PCB + bent antenna, rotated clockwise: (a) picture of the target, as seen from the antennas, (b) peak-amplitude vs. angle for VV and VH; outer axis labels are in degrees; inner labels are in dBm.

Comparing Figs. 30 and 31 against Figs. 28 and 29, elongation of the PCB (and the copper trace across it) does not generate a stronger nonlinear response: the angular pattern squeezes in (i.e. it is generally reduced) and it now displays a main lobe near 90º-120º (vs. approximately-equal front and back lobes in the earlier plots). Further elongation of the PCB, as in Fig. 32, produces three approximately-equal lobes. Fig. 33 appears to be a warped version of Fig. 32, with the lobe near 210º suppressed.

While none of Figs. 28–33 closely match Figs. 6–27, the data of Fig. 28 resembles that of Fig. 9 (rotated by 90º) and Fig. 11 resembles a rotated and attenuated version of Fig. 30. The data suggest that this target-assembly could be modified to more faithfully replicate the response-vs.-angle patterns of real electronic devices, but more extensive tweaking of the assembly is required to achieve a close match.

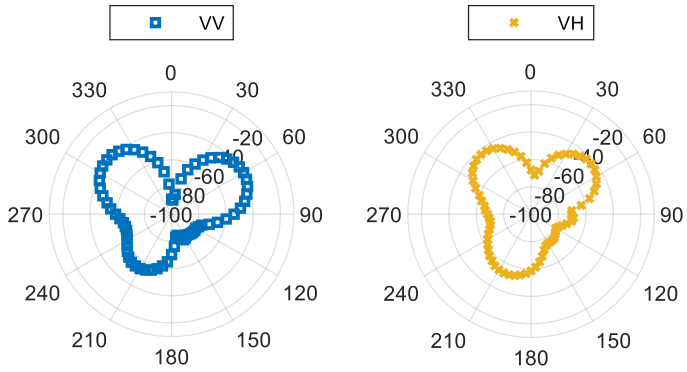

Fig. 32. NLJ + 8-inch PCB + straight antenna, rotated clockwise: (a) picture of the target, as seen from the antennas, (b) peak-amplitude vs. angle for VV and VH; outer axis labels are in degrees; inner labels are in dBm.

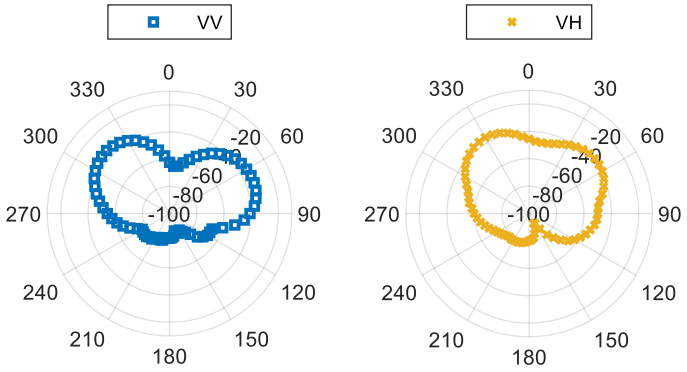

Fig. 33. NLJ + 8-inch PCB + bent antenna, rotated clockwise: (a) picture of the target, as seen from the antennas, (b) peak-amplitude vs. angle for VV and VH; outer axis labels are in degrees; inner labels are in dBm.

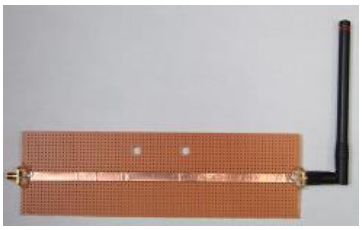

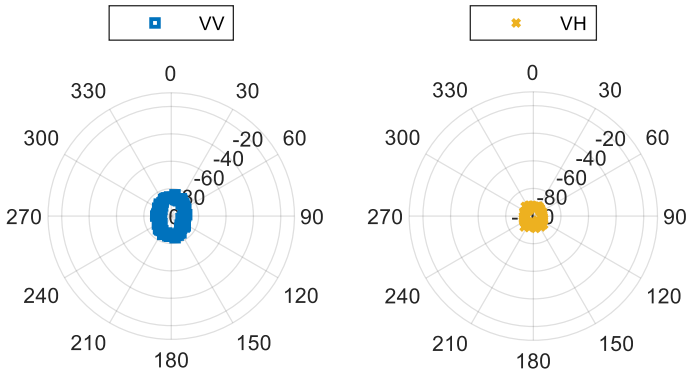

Fig. 34. Open-circuit + 8-inch PCB + bent antenna, rotated clockwise: (a) picture of the target, as seen from the antennas, (b) peak-amplitude vs. angle for VV and VH; outer axis labels are in degrees; inner labels are in dBm.

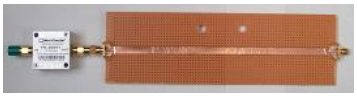

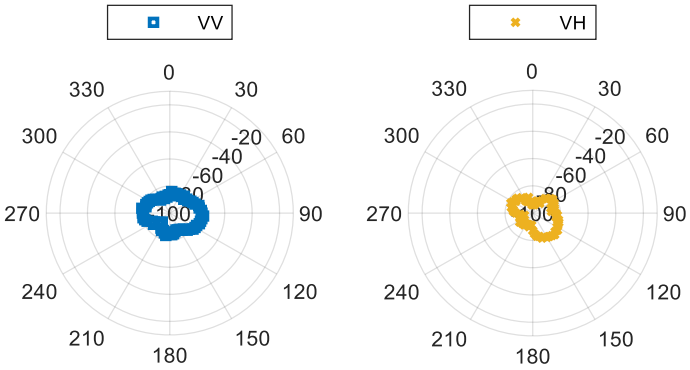

Fig. 35. NLJ + 8-inch PCB, without antenna, rotated clockwise: (a) picture of the target, as seen from the antennas, (b) peak-amplitude vs. angle for VV and VH; outer axis labels are in degrees; inner labels are in dBm.

When the FK-3000+ was removed from the assembly, as in Fig. 34, the target response dropped into the noise. This result confirms that the frequency-doubler is the original source of the harmonics (i.e. it is the nonlinear junction being detected). When the antenna was removed, as in Fig. 35, the response dropped significantly but the target was still detectable; this behavior matches that of the radios and the RC-tank transmitters.

Table III summarizes the data recorded from the NLJ/PCB/antenna assembly. In general, the standard-deviation of the assembly is much greater than that recorded from the targets in both the "clock-rotation" and "top-spin" experiments. Since the deviation generally increases with the length of the PCB, it is likely that a shorter PCB (1 inch or less) would better replicate the harmonic responses of electronic devices.

	radar orientation & statistic:			
target:	**VV, mean**	**VV, SD**	**VH, mean**	**VH, SD**
no target -- empty platform	–91 dBm	1 dB	–91 dBm	1 dB
NLJ + 2-in PCB + straight antenna	–52 dBm	14 dB	–51 dBm	12 dB
NLJ + 2-in PCB + bent antenna	–50 dBm	11 dB	–51 dBm	12 dB
NLJ + 4-in PCB + straight antenna	–67 dBm	13 dB	–66 dBm	13 dB
NLJ + 4-in PCB + bent antenna	–65 dBm	16 dB	–61 dBm	13 dB
NLJ + 8-in PCB + straight antenna	–60 dBm	15 dB	–60 dBm	11 dB
NLJ + 8-in PCB + bent antenna	–59 dBm	18 dB	–58 dBm	17 dB
open + 8-in PCB + bent antenna	–88 dBm	2 dB	–93 dBm	1 dB
NLJ + 8-in PCB + open circuit	–84 dBm	4 dB	–86 dBm	5 dB

Table III. Mean and standard-deviation; range-profile peaks; hardware-modeling "clock-rotation" experiment.

4. CONCLUSIONS

In this preliminary study, six electronic devices were illuminated with radar waves and harmonics of those waves were captured for different orientations of the target -- at 72 discrete positions within a full 360º rotation. The data generally indicate that, when each target is rotated "like a clock," there is a very strong link between rotation-angle and strength of the response. None of the angular dependencies appears to be perfectly symmetric nor closely matches that of another device; thus, it is possible that the response-vs.-angle characteristic may be used as the basis for a signature used to identify such devices.

Data captured for vertical and horizontal polarizations of the radar antennas indicate that nonlinear response is maximized when the orientation of the radar's transmit antenna matches the orientation of the RF device's (intended, external) antenna. Data collected when the targets are "spun like a top" indicate that some wide printed-circuit-boards do contribute significantly to a target's nonlinear response.

An assembly of a nonlinear junction + PCB + antenna replicates some parts of the harmonic responses produced by commercial electronic devices: rough received-signal levels and signal strength preferential to the alignment of the target antenna with the radar transmit antenna. Warping of the response-vs.-angle pattern with different lengths of PCB indicates that it may be possible to tailor the assembly to more closely match the response-vs.-angle patterns of real electronics.

REFERENCES

[1] H. T. Hayvaci, M. Shahi, H. Ilbegi and I. S. Yetik, "A linear model for classification of electronic devices using harmonic radar," *IEEE Trans. Aerosp. Electron. Sys.,* vol. 57, no. 6, pp. 3614-3622, Dec. 2021.

[2] A. Abdelnour, A. Lazaro, R. Villarino, D. Kaddour, S. Tedjini and D. Girbau, "Passive harmonic RFID system for buried assets localization," *MDPI Sensors,* vol. 18, no. 3635, pp. 1-21, Oct. 2018.

[3] S. M. Aguilar and T. M. Weller, "Tunable harmonic re-radiator for sensing applications," in *Proc. IEEE MTT-S Int. Microw. Symp.*, Boston, MA, June 2009.

[4] M. Bouthinon, J. Gavan and F. Zadworny, "Passive microwave transposer, frequency doubler for detecting the avalanche victims," in *Proc. Europ. Microw. Conf.*, Warszawa, Poland, Sept. 1980.

[5] E. A. Capaldi, A. D. Smith, J. L. Osborne, S. E. Fahrbach, S. M. Farris, D. R. Reynolds, A. S. Edwards, A. Martin, G. E. Robinson, G. M. Poppy and J. R. Riley, "Ontogeny of orientation flight in the honeybee revealed by harmonic radar," *Nature,* vol. 403, p. 537–540, Feb. 2000.

[6] X. Gu, N. S. Nikhil, L. Guo, S. Hemour and K. Wu, "Diplexer-based fully passive harmonic transponder for sub-6-GHz 5G-compatible IoT applications," *IEEE Trans. Microw. Theory Techn.,* vol. 67, no. 5, pp. 1675-1687, May 2019.

[7] A. Lavrenko, S. Pawson and J. Cavers, "On the use of additional transmitters for increasing detection range in harmonic radar," in *Proc. Int. Conf. Signal Proc. Comm. Sys.*, Gold Coast, Australia, Dec. 2019.

[8] T. Harzheim, M. Mühmel and H. Heuermann, "A SFCW harmonic radar system for maritime search and rescue using passive and active tags," *Int. J. Microw. Wireless Tech.,* pp. 1-17, Mar. 2021.

[9] G. J. Mazzaro, A. F. Martone and D. M. McNamara, "Detection of RF electronics by multitone harmonic radar," *IEEE Trans. Aerosp. Electron. Sys.,* vol. 50, no. 1, Jan. 2014.

[10] N. Nourshamsi, S. Vakalis and J. A. Nanzer, "Joint detection of human and object motion using harmonic micro-doppler radar and harmonic tags," *IEEE Ant. Wireless Propag. Lett.,* vol. 19, no. 6, pp. 930-934, June 2020.

[11] V. Palazzi, F. Alimenti, P. Mezzanotte, G. Orecchini and L. Roselli, "Zero-power, long-range, ultra low-cost harmonic wireless sensors for massively distributed monitoring of cracked walls," in *Proc. IEEE MTT-S Int. Microw. Symp.*, Honololu, HI, June 2017.

[12] D. Dardari, "Detection and accurate localization of harmonic chipless tags," *EURASIP J. Adv. Signal Process.,* vol. 77, pp. 1-13, Aug. 2015.

[13] G. L. Lovei, I. A. N. Stringer, C. D. Devine and M. Cartellieri, "Harmonic radar: A method using inexpensive tags to study invertebrate movement on land," *New Zealand J. Ecology,* vol. 21, no. 2, pp. 187-193, 1997.

[14] A. Mishra, W. McDonnell, J. Wang, D. Rodriguez and C. Li, "Intermodulation-based nonlinear smart health sensing of human vital signs and location," *IEEE Access,* vol. 7, pp. 158284-158295, Oct. 2019.

[15] X. Hui and E. C. Kan, "Radio ranging with ultrahigh resolution using a harmonic radio-frequency identification system," *Nature Electronics,* vol. 2, pp. 125-131, Mar. 2019.

[16] S. Mondal, D. Kumar and P. Chahal, "Recent advances and applications of passive harmonic RFID systems: A review," *MDPI Micromachines,* vol. 12, no. 420, pp. 1-22, Apr. 2021.

[17] A. Lazaro, R. Villarino and D. Girbau, "A passive harmonic tag for humidity sensing," *Int. J. Ant. Propag.,* vol. 2014, pp. 1-11, July 2014.

[18] A. Martorell, J. Raoult, R. Marijon and L. Chusseau, "RF front-ends nonlinearity characterization using reflected power," *IEEE Trans. Electromag. Compat.,* vol. 59, no. 6, pp. 1925-1931, Dec. 2017.

[19] K. A. Gallagher, R. M. Narayanan, G. J. Mazzaro, A. F. Martone and K. D. Sherbondy, "Static and moving target imaging using harmonic radar," *MDPI Electronics,* vol. 6, no. 2, Apr. 2017.

[20] F. T. Ulaby and U. Ravaioli, Fundamentals of applied electromagnetics, Upper Saddle River, NJ: Pearson Education, Inc., 2015.

[21] C. A. Balanis, Antenna theory: Analysis and design, Hoboken, NJ: John Wiley & Sons, Inc., 2005.